

Metastability of a periodic network of threads: what are the shapes of a knitted fabric ?

Jérôme Crassous

*Univ Rennes, CNRS, IPR (Institut de Physique de Rennes) - UMR 6251, F-35000 Rennes, France**

Samuel Poincloux

*Department of Physical Sciences, Aoyama Gakuin University,
5-10-1 Fuchinobe, Sagamihara, Kanagawa 252-5258, Japan*

Audrey Steinberger

Univ Lyon, ENS de Lyon, CNRS, Laboratoire de Physique, F-69342 Lyon, France

(Dated: October 24, 2024)

Knitted fabrics are metamaterials with remarkable mechanical properties, such as extreme deformability and multiple history-dependent rest shapes. This letter shows that those properties may stem from a continuous set of metastable states for a fabric free of external forces. This is evidenced through experiments, numerical simulations and analytical developments. Those states arise from the frictional contact forces acting in the braid zone where the threads interlace and follow a line in the configuration space accurately described by a 2D-elastica model. The friction coefficient sets a terminal point along this line, and the continuous set of metastable states is obtained by varying the braid inclination while contact forces remain on the friction cone.

Assemblies of long, flexible, and intertwined fibers with frictional contacts are materials involved in various phenomena, including surgical or shoe knots [1, 2], nests and self-assembled natural structures [3, 4], nonwoven fabrics with a wealth of applications [5], or the degradation of ancient manuscripts [6]. Despite being essential for most applications, the mechanical response of fiber assemblies is intrinsically non-linear, dissipative, and history-dependent, stemming from the fibers' slenderness and the frictional contacts. Providing quantitative mechanical predictions for the assembly from the properties of the fibers remains a theoretical and numerical challenge, with recent advances made in simplified situations with tight geometries [7–9]. One particular class of ordered fiber assemblies, textiles, have tremendous industrial importance in manufacturing [10] or geo-engineering [11]. They also recently gained a renewed interest as metamaterials with extensive programmability [12, 13] for emerging soft robotics and smart textile applications [14, 15]. However, the prediction of basic properties, like the rest shape of a knitted fabric given the length by stitch of its constitutive yarn, is an old but still open question [16, 17] even though a reproducible state can be achieved after repeated multidirectional stretching [18]. One possible way of progress may emerge from yarn-level simulation of knitted fabrics for which the computer graphics community made enormous progress [19–21], but the dynamics usually rely on viscous dissipative forces at the contacts, ill-adapted to capture rest shapes arrested by dry friction. Nonetheless, recent numerical advances allow the combination of large fiber displacements with frictional interactions [22–25] and open the way to explore quan-

titatively the mechanics and stability of frictional fiber assemblies [26]. The complex geometry of the contact zones between fibers makes exact theoretical modeling extremely complicated. In this letter, we show that a simplified description of these zones can faithfully reproduce the rest shapes of a knitted fabric. The postulate of a single form of equilibrium must be abandoned. Even with zero external stresses ($\sigma^{\text{ext}} = 0$), the solid friction between the threads stabilizes the materials in various metastable states depending on the system's history.

In this study, we use a Jersey stitch knit, which is both simple and widely used. It consists of a single yarn forming interlocked loops as in Fig. 1(a). Experimentally, we make a knitted fabric of 70×70 stitches from a polyamide (Nylon) thread (Madeira Monofil n°40, $E = 1.05$ GPa, $\mu = 0.5$) of diameter $d = 0.155$ mm. The length of thread per stitch is $\ell = 9.7$ mm. The central $N \times N$ stitches ($N = 50$) are attached to a biaxial tensile machine (Fig. 1.b), where the spacing Δx along the courses and Δy along the wales can be varied by stepper motors. The forces per row $f_x := F_x/N$ and columns $f_y := F_y/N$ are measured using strain gauge force sensors. The network's periodicity (ℓ_x, ℓ_y) is obtained from images recorded with a camera. The network is also studied using numerical simulations based on Discrete Elastic Rods (DER) coupled with dry contacts with a friction coefficient μ [25, 27]. Threads are decomposed into segments of circular cylinders connected by springs, which account for the elastic forces of traction, flexion, and torsion. A mesh comprises 3 rods as shown in fig 1.c. The endpoints of these 3 wires are constrained to the $\pm \ell_x/2$ or $\pm \ell_y/2$ planes. Periodic boundary conditions in terms of positions and forces are applied at the junctions between the strands: for example, the strands 1 and 2 satisfy $\mathbf{r}_{2a} - \mathbf{r}_{1a} = \ell_y \mathbf{e}_y$, $\alpha_{2a} = \alpha_{1a}$, $\mathbf{r}'_{2a} = \mathbf{r}'_{1a}$ and $\mathbf{r}''_{2a} = \mathbf{r}''_{12}$. α is

* jerome.crassous@univ-rennes.fr

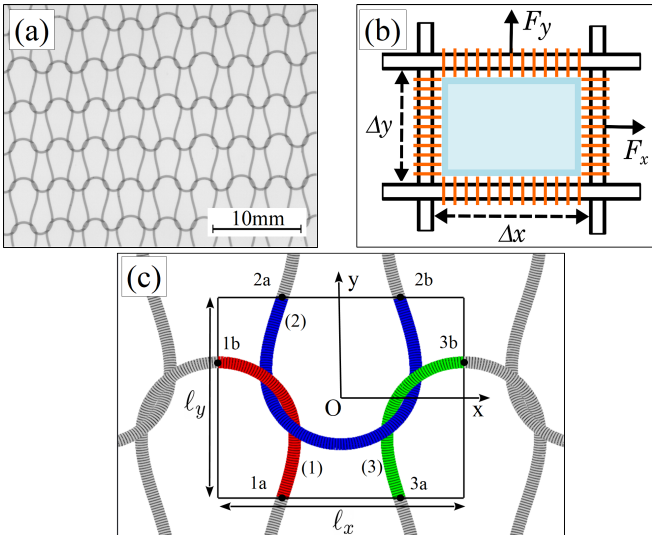


FIG. 1. (a) Photo of a Jersey stitch knit. (b) Experimental set-up. The knitted fabric (light blue) is attached with metallic staples (orange) that can freely slide over 4 cylindrical bars linked to a biaxial tensile machine. (c) Geometry and numerical model. A rectangular cell of size $\ell_x \times \ell_y$ is composed of 3 threads (1), (2) & (3). Segments of cylinders composing the threads are colored. Dots 1a, 1b,... are the endpoints of the different threads, which are constrained to be on the cell boundaries with periodic boundary conditions.

the torsion angle, ' and '' are the 1st and 2nd derivatives with respect to the curvilinear abscissa s . Conditions on the derivatives ensure the continuity of the forces and moments.

We identify the rest states at $\sigma^{\text{ext}} = 0$ as follows. Experimentally, the knitted fabric is stretched to an initial state $(\Delta x_0, \Delta y_0)$, then Δx and Δy are varied to reduce $f := (f_x^2 + f_y^2)^{1/2}$ until it becomes lower than $f_{\text{min}} = 8$ mN. Numerically, starting from a given stretched configuration, the stitch length is varied by $\delta \ell_i = -\lambda f_i$, with $i = x, y$ and λ a numerical constant, until the force is smaller to a given threshold. Fig.2 shows the mesh sizes obtained following this experimental and numerical protocol. Firstly, the rest shape of the knitted fabric is not uniquely defined and is strongly dependent on the initial state. Secondly, these shapes belongs to a curve which is an attractor in the space of (ℓ_x, ℓ_y) configurations. This curve ends at a terminal point $T := (\ell_{xT}, \ell_{yT})$. A knit verifying $\ell_y > \ell_{yT}$ or $\ell_x < \ell_{xT}$ is impossible without external forces. Finally, the experimental and numerical data agreement is very satisfactory: modeling a polyamide thread with an elastic fiber without cross-sectional deformations is a reasonable hypothesis. Plastic deformations occurring during knitting, leading to stress-free yarn no longer ideally rectilinear, underlie the observed differences.

To describe the set of rest states, we consider the elastic energy $E(\ell_x, \ell_y) = E^{(b)} + E^{(t)} + E^{(s)}$, with respectively the bending, twisting and stretching energy. It is obtained from DER simulations for a unit cell of fric-

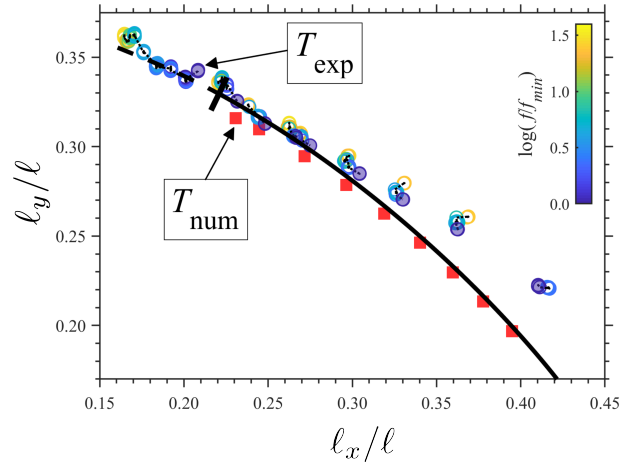


FIG. 2. Relaxed configurations of a knitted fabrics ($\ell/d = 62.5$, $\mu = 0.5$). (open circles): Experimental configurations during relaxation, color-coded by $\log(f/f_{\text{min}})$. The dotted lines are guidelines. (filled disks): Relaxed, experimental configurations; (red squares): Configurations obtained from DER simulations. There are no relaxed configurations above or to the left of the terminal points T , noted T_{exp} (resp. T_{num}) for experimental (resp. numerical) data. (black line): Possible configurations expected from a 2D-elastic model with no applied stress, with the predicted terminal point separating the accessible (plain) and forbidden (dashed) regions.

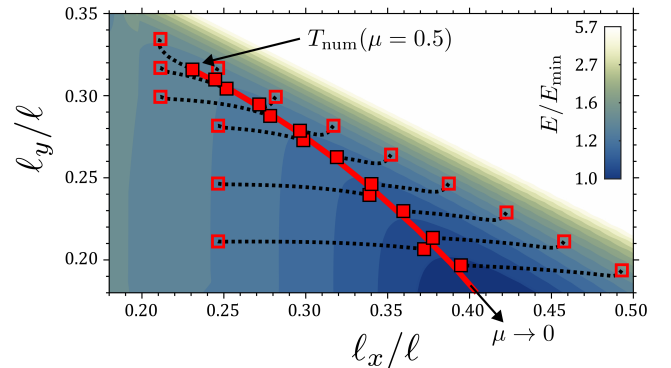


FIG. 3. Elastic energy E (color bar) for cells of imposed size made of frictionless threads ($\mu = 0$, $\ell/d = 62.5$). The energy is normalized by E_{min} , the minimum energy reached by a frictionless stitch without external stress. (Dotted lines): Relaxations of fabric with frictional thread ($\mu = 0.5$) between an initial configuration (open red square) and a relaxed configuration (filled red square). $T_{\text{num}}(\mu = 0.5)$ is the terminal point. (Plain red curve): Relaxation of a fabric, initially at $T_{\text{num}}(\mu = 0.5)$, when μ is gradually decreased.

tionless fabric (Fig. 3). A valley that descends towards small ℓ_y and large ℓ_x separates the traction zones (large ℓ_x or ℓ_y) from the compressive zones (small ℓ_x or ℓ_y). The knitted fabric relaxes its bending energy by aligning its yarns parallel to \mathbf{e}_x . The milder slope in this energy landscape acts as an attractor line for frictional knitted

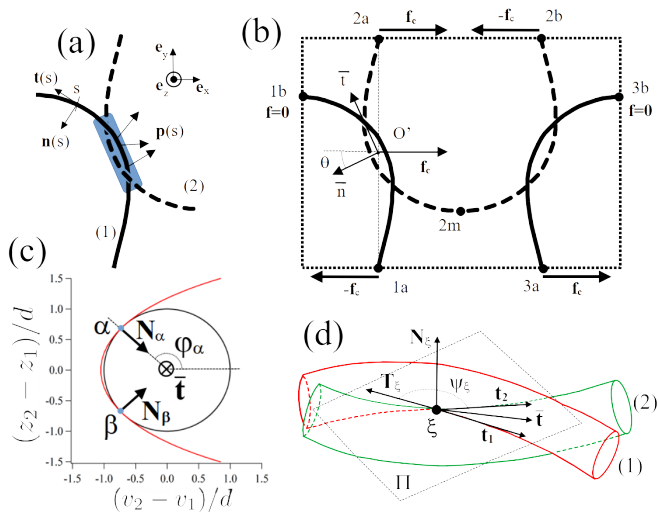


FIG. 4. (a) Contact forces $\mathbf{p}(s)$ acting in the braid zone (blue rectangle). (b) Forces acting on one mesh for a rest state $\sigma^{\text{ext}} = 0$. The total forces on each side is 0, and the internal forces acting on threads are 0 or $\pm \mathbf{f}_c$. The points (1a) and (2a) are on the vertical line of middle point O' , and $\bar{\mathbf{t}}$ is the braid direction. (c) (Red line): Projection of the vector $\mathbf{r}_2 - \mathbf{r}_1$, joining the centerlines, on the planes perpendicular to $\bar{\mathbf{t}}$. v is the coordinate along an axis of direction $-\bar{\mathbf{n}} := \bar{\mathbf{t}} \times \mathbf{e}_z$. The circle is of unit radius. Contact occurs in two points α and β (blue dots) that makes angles φ_α and $\varphi_\beta = -\varphi_\alpha$ with the $z = 0$ plane. (d) Orientations of the contact force at a contact point ξ . The plane Π containing \mathbf{t}_1 and \mathbf{t}_2 is normal to \mathbf{N}_ξ . \mathbf{T}_ξ is the direction of the tangential contact force, which makes an angle Ψ_ξ with $\bar{\mathbf{t}}$.

fabrics with $\mu \neq 0$. Stretched or compressed fabrics relax (Fig. 3, dotted lines) and stop close to the valley floor. Due to the non-conservative nature of frictional forces, the trajectories obtained at $\mu \neq 0$ are not maximal slopes of $E(\ell_x, \ell_y)$.

We then obtain the rest configurations and terminal points T_{num} as functions of μ (Fig. 3, continuous red line). The endpoints $T_{\text{num}}(\mu)$ sit along a line on the valley floor and go down the milder slope as μ decreases. This line is the attractor for the relaxing trajectories which stop in its vicinity. As $\mu \rightarrow 0$, this line ends because contacts between non-successive rows occur, but this limit is not discussed here.

Therefore, describing the set of metastable configurations requires understanding i) the shape of the friction-independent valley; ii) how the friction μ controls the position of the terminal point T on the line of milder slope.

Interactions between the yarns take place in the braid where they become entangled, creating both normal and tangential forces to the threads. To describe this zone, schematically depicted in Fig. 4.a, we introduce the curvilinear abscissa s along the centerline of thread (1), and $\mathbf{p}(s)$ the linear density of contact force exerted by (2) on (1). Because friction is present, $\mathbf{p}(s)$ is not necessarily

aligned to the normal vector $\mathbf{n}(s)$. We define

$$\mathbf{f}_c = \int_{s_{in}}^{s_{out}} \mathbf{p}(s) ds \quad (1)$$

the resultant of contact forces with s_{in} the entrance of the contact zone: $\mathbf{p}(s_{in}) \neq 0$ and $\mathbf{p}(s) = 0$ for $s < s_{in}$, with reciprocal definition for s_{out} . For any rest state $\sigma^{\text{ext}} = 0$, the sum of total forces acting on each side of the unit cell must be 0 (see Fig.4.b). Along the row, the external forces acting on points (1b) and (3b) vanish $\mathbf{f}_{1b} = \mathbf{f}_{3b} = 0$, while along the column $\mathbf{f}_{2a} + \mathbf{f}_{2b} = \mathbf{f}_{1a} + \mathbf{f}_{3a} = 0$. Periodicity and symmetry along the y axis imply, $\mathbf{f}_{1a} = -\mathbf{f}_{2a}$ and $\mathbf{f}_{1a} = f_{1a} \mathbf{e}_x$. Finally, equilibrium of thread (1) with $\mathbf{f}_{1a} + \mathbf{f}_{1b} + \mathbf{f}_c = 0$ results in an horizontal contact force $\mathbf{f}_c \cdot \mathbf{e}_y = 0$ and $\mathbf{f}_{1a} = -\mathbf{f}_c$. The results of the DER simulations fulfilled all those requirements.

Let s_c be the arbitrary abscissa of contact at which \mathbf{f}_c is applied. In the limit $d/\ell \ll 1$, we consider the bi-dimensional problem of finding the value of $f_c := \|\mathbf{f}_c\|$ such that the 2D elastic curve $\mathbf{r}(s)$ representing the strand (1) is at equilibrium. The curve must satisfy the applied external force \mathbf{f}_c at $s = s_c$ and $-\mathbf{f}_c$ at $s = s_{1a} = 0$, and verifying $dy/ds = 0$ at $s = s_{1b} = \ell/4$ and $(\mathbf{r}(s_c) + (d/2)\mathbf{n}(s_c) - \mathbf{r}(0)) \cdot \mathbf{e}_x = 0$. The last condition imposes contacts between the two threads in O' . Note that the threads actually touch in two points (Fig.4.c), but the distance between the centerlines in O' is typically $1.03 d \simeq d$, and the distance between contact points is $\ll \ell$, validating the simplifying assumption of a unique contact point at s_c . There are no explicit solutions to this 2D-elastica problem, and we solved it numerically. For each arbitrary value of s_c we obtain f_c , $\mathbf{r}(s_c)$, $\mathbf{n}(s_c)$, and braid inclination $\tan(\theta) := -(dy/dx)(s_c)$. Using symmetries of the cell, we obtain:

$$\mathcal{L}_x(s_c) = \left(4[\mathbf{r}(s_c) - \mathbf{r}(\ell/4)] + 2d \mathbf{n}(s_c) \right) \cdot \mathbf{e}_x \quad (2a)$$

$$\mathcal{L}_y(s_c) = \left(2[\mathbf{r}(s_c) - \mathbf{r}(0)] + d \mathbf{n}(s_c) \right) \cdot \mathbf{e}_y \quad (2b)$$

$(\mathcal{L}_x(s_c), \mathcal{L}_y(s_c))$ is the parametric curve in the plane (ℓ_x, ℓ_y) shown on Fig.2. All the rest states stand very close to this parametric curve, from a simple 2D approximation of the full 3D problem.

All configurations of the parametric curve verify $\mathbf{f}_c \cdot \mathbf{e}_y = 0$. However, the tangential and normal components of contact forces are linked by Coulomb's friction law. This imposes a maximal braid inclination $\tan(\theta_M)$, that sets the terminal point $T(\mu)$. The position of this point is predicted by considering the details of the contact force distribution $\mathbf{p}(s)$.

The braid comprises two twisted fibers in a geometry similar to the one occurring in knots where the threads are twisted of n turns. The cases $n = 1$ (3_1 knot) [28, 29], $n = 2$ (5_1 knot) [29] and $n \gg 1$ [30] have been considered previously. Threads in the braid are approximately a helix contacting in a few points. It seems that our braid with $n = 1/2$ has not been previously considered, but it

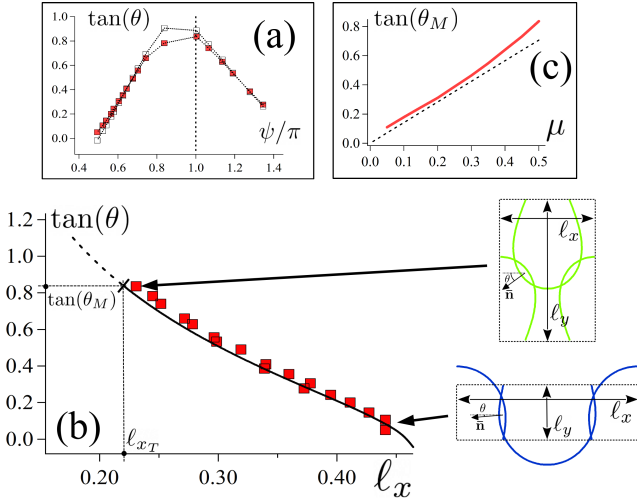


FIG. 5. (a) For rest states with $\mu = 0.5$, braid inclination $\tan(\theta)$ against tangential forces direction ψ/π . (Filled square): $\tan(\theta)$ measured from DER. (Open square): right term of (6) with φ from DER. (Dashed line): approximated position of the maximum at $\psi = \pi$. (b) Braid inclination $\tan(\theta)$ vs cell dimension ℓ_x . (Filled squares): DER rest states obtained with $\mu = 0.5$. (Line): $\tan(\theta)$ vs \mathcal{L}_x of the 2D-Elastica model. (Black dash): theoretical terminal point. (Insets): threads centerlines for rest states with $\tan(\theta) \simeq 0$ and $\tan(\theta) \simeq \tan(\theta_M)$. Dashed rectangles are the meshes of sizes $\ell_x \times \ell_y$. (c) (Red line): $\tan(\theta_M)$ versus μ from DER. (Dash line): Eq.(7) with $\varphi = 3\pi/4$.

exhibits a very similar behavior. The threads have nearly helical shapes twisted around a common line of direction $\bar{\mathbf{t}} = [\mathbf{t}_1(s_1) + \mathbf{t}_2(s_2)] / \|\mathbf{t}_1(s_1) + \mathbf{t}_2(s_2)\|$, where \mathbf{t}_1 and \mathbf{t}_2 are threads (1) and (2) centerlines' tangent vector. The figure 4.c represents the relative position $\mathbf{r}_2(s_2) - \mathbf{r}_1(s_1)$ of the threads, where $\mathbf{r}_1(s_1)$ and $\mathbf{r}_2(s_2)$ are the projections of the centerlines on the plane perpendicular to $\bar{\mathbf{t}}$. With the fibers contacting in two points α and β :

$$\mathbf{f}_c = \int \mathbf{p}(s) ds = \sum_{\xi=\alpha,\beta} [f_\xi^{(n)} \mathbf{N}_\xi + f_\xi^{(t)} \mathbf{T}_\xi] \quad (3)$$

with \mathbf{N}_ξ the contact point's normal vector, \mathbf{T}_ξ the orientation of the tangential contact forces (Fig.4(d)), and $f_\xi^{(n)}$ and $f_\xi^{(t)}$ the normal and tangential forces. For all equilibrium configurations, we found $f_\alpha^{(n)} = f_\beta^{(n)} := f^{(n)}$ and $(\mathbf{N}_\alpha + \mathbf{N}_\beta) \cdot \mathbf{e}_z = 0$. Noting φ_ξ the angle between \mathbf{N}_ξ and $z = 0$ (Fig.4.c), we have $\varphi_\alpha = -\varphi_\beta := \varphi$, with $\varphi \simeq 3\pi/4$ for each relaxed configuration.

When the meshes are steadily deformed, the threads in the braid slide. The friction is then fully mobilized, and $f_\xi^{(t)} = \mu f_\xi^{(n)}$. Since $\mathbf{N}_\xi \cdot \mathbf{t}_i(s_\xi) = 0$ for the two threads $i = 1, 2$, \mathbf{N}_ξ is perpendicular to the plane containing $\mathbf{t}_1(s_\xi)$ and $\mathbf{t}_2(s_\xi)$. \mathbf{T}_ξ belongs to this plane, and we may write:

$$\mathbf{T}_\xi = \cos(\psi_\xi) \bar{\mathbf{t}} + \sin(\psi_\xi) [\bar{\mathbf{t}} \times \mathbf{N}_\xi] \quad (4)$$

where ψ_ξ is the angle between \mathbf{T}_ξ and $\bar{\mathbf{t}}$ (Fig.4.d). Using Eq.(3) and Eq.(4), we may calculate \mathbf{f}_c . With $\varphi_\alpha = -\varphi_\beta$, the equilibrium conditions $\mathbf{f}_c \cdot \mathbf{e}_z = 0$ leads to $\psi_\alpha = -\psi_\beta := \psi$, and finally:

$$\mathbf{f}_c = 2f^{(n)} \times \left(\mu \cos(\psi) \bar{\mathbf{t}} + [\cos(\varphi) + \mu \sin(\varphi) \sin(\psi)] \bar{\mathbf{n}} \right) \quad (5)$$

With $\bar{\mathbf{t}} \cdot \mathbf{e}_y = \cos(\theta)$, the equilibrium condition for a $\sigma^{\text{ext}} = 0$ configuration, $\mathbf{f}_c \cdot \mathbf{e}_y = 0$, writes:

$$\tan(\theta) = \frac{\mu \cos(\psi)}{\cos(\varphi) + \mu \sin(\varphi) \sin(\psi)} \quad (6)$$

For a given μ , and because φ is roughly constant, variation of $\tan(\theta)$ are driven by variation of the tangential forces direction ψ . Fig.5(a) shows $\tan(\theta)$ versus ψ for the relaxed states obtained by DER simulations and confirms that (6) holds. The tangential forces at the two contact points α and β rotate on either side of the braid axis $\bar{\mathbf{t}}$. The effect of those rotations is to vary the amplitude of the total friction force along the $\bar{\mathbf{t}}$ axis, even if individual friction forces always evolve at the Coulomb threshold.

The inclination of the braid is a fundamental quantity that controls the cell size (ℓ_x, ℓ_y). Fig.5(b) shows the relation between $\tan(\theta)$ and ℓ_x (similar relation may be obtained for ℓ_y) for the 2D-elasticity model and DER data. The way increasing the inclination $\tan(\theta)$ shrinks ℓ_x (Fig.5(b), insets) is well captured by our 2D-elasticity model.

The existence and position of the terminal point $T = (\ell_{xT}, \ell_{yT})$ are predicted by Eq.(6): $\tan(\theta)$ is bounded by some maximal value $\tan(\theta_M)$, the relation between $\tan(\theta)$ and ℓ_x (respectively ℓ_y) imposes a minimum (resp. maximum) value ℓ_{xT} (resp. ℓ_{yT}). With φ constant, $\tan(\theta)$ is maximal for a rotation $\psi = \pi + \arcsin(\mu \tan(\varphi)) \simeq \pi$ for $\mu \ll 1$ and $\varphi \simeq 3\pi/4$ as shown in Fig.5.a. This maximal value of θ is obtained when the frictional forces are roughly aligned with the common tangent of the centerline. Approximating $\psi = \pi$ in Eq.(6), we finally obtain for small μ :

$$\tan \theta \leq \tan(\theta_M) := \frac{\mu}{|\cos(\varphi)|} \quad (7)$$

where θ_M is the maximal value of θ . The simplified prediction of Eq.(7) is verified by confronting, for different values of μ , the predicted values of $\tan(\theta_M)$ with a constant $\varphi = 3\pi/4$ and the ones measured from DER (Fig.5.c).

To summarize, in the configuration space (ℓ_x, ℓ_y) , any rest knitted Jersey lies on a curve given by Eq.(2) which does not depend on μ . However, for a given value of μ , only a subset of this curve is possible because of Coulomb's friction law. This subset increases with friction and ends at a point $T(\mu)$ for which $\theta = \theta_M(\mu)$ (fixed by Eq.(7)).

Our study rationalizes the $\sigma^{\text{ext}} = 0$ rest state of a periodic yarn assembly. They are not unique but form a

continuous subset, bounded by a terminal point T , in the space of possible periodic configurations (ℓ_x, ℓ_y) of a knitted fabric. Those findings have many implications. The configuration corresponding to T would be the reproducible shape of a $\sigma^{\text{ext}} = 0$ knitted fabric, accessible through successive stretching cycles along y , even if metastability makes other rest shapes possible. The existence of a continuum of relaxed states has important consequences for the macroscopic mechanical properties. The restoring forces are, therefore, weak over a wide range of the configuration space. Knitted fabrics are soft objects for deformations that remain in this zone but are relatively rigid when we move away from it. Finally, variations in aspect ratios mean that the area per stitch $\ell_x \times \ell_y$ can be varied at zero external force. A flat knitted fabric can thus be stretched to cover a surface with non-zero Gaussian curvature without any external forces being applied. This study can also serve as a ground basis for exploring further the mechanics of knitted fabrics or, more generally, of periodic three-dimensional struc-

tures [31]. The numerical and theoretical models can be adapted to different knitting topology [13], but also for fibers closer to applications by modifying the elastic properties of the rod or smaller aspect ratio ℓ/d . The methods introduced here can also be adapted to explore the role of friction in the force vs. strain responses of textiles, including hysteresis [12] and slip-induced fluctuations [32].

ACKNOWLEDGMENTS

A.S. thanks D. Le Tourneau and P. Metz for building the biaxial tensile machine. J.C. acknowledges CNRS-Physique for hosting in delegation. S.P. acknowledges financial support from the Japanese Society for the Promotion of Science as a JSPS International Research Fellow. This work has been supported by Agence Nationale de la Recherche Grant ANR-23-CE30-0015.

-
- [1] Paul Johanss, Changyeob Baek, Paul Grandgeorge, Samia Guerid, Shawn A Chester, and Pedro M Reis. The strength of surgical knots involves a critical interplay between friction and elastoplasticity. *Sci. Adv.*, 9(23):eadg8861, 2023.
- [2] Christopher A Daily-Diamond, Christine E Gregg, and Oliver M O’Reilly. The roles of impact and inertia in the failure of a shoelace knot. *Proc. R. Soc. A*, 473(2200):20160770, 2017.
- [3] Nicholas Weiner, Yashraj Bhosale, Mattia Gazzola, and Hunter King. Mechanics of randomly packed filaments—the “bird nest” as meta-material. *J. Appl. Phys.*, 127(5), 2020.
- [4] Gautier Verhille, Sébastien Moulinet, Nicolas Vandenberghe, Mokhtar Adda-Bedia, and Patrice Le Gal. Structure and mechanics of aegagropilae fiber network. *Proc. Natl. Acad. Sci. U.S.A.*, 114(18):4607–4612, 2017.
- [5] Wilhelm Albrecht, Hilmar Fuchs, and Walter Kittelmann. *Nonwoven fabrics: raw materials, manufacture, applications, characteristics, testing processes*. John Wiley & Sons, 2006.
- [6] Caroline Vibert, Anne-Laurence Dupont, Justin Dirrenberger, Raphaël Passas, Denise Ricard, and Bruno Fayolle. Relationship between chemical and mechanical degradation of aged paper: fibre versus fibre–fibre bonds. *Cellulose*, pages 1–19, 2024.
- [7] Samuel Poincloux, Tian Chen, Basile Audoly, and Pedro M. Reis. Bending response of a book with internal friction. *Phys. Rev. Lett.*, 126:218004, May 2021.
- [8] Antoine Seguin and Jérôme Crassous. Twist-controlled force amplification and spinning tension transition in yarn. *Phys. Rev. Lett.*, 128(7):078002, 2022.
- [9] Julien Chopin, Animesh Biswas, and Arshad Kudrolli. Energetics of twisted elastic filament pairs. *Phys. Rev. E*, 109:025003, Feb 2024.
- [10] Andrew Craig Long. *Design and manufacture of textile composites*. Elsevier, 2005.
- [11] Robert Koerner. *Geotextiles: from design to applications*. Woodhead Publishing, 2016.
- [12] Samuel Poincloux, Mokhtar Adda-Bedia, and Frédéric Lechenault. Geometry and elasticity of a knitted fabric. *Phys. Rev. X*, 8:021075, Jun 2018.
- [13] Krishma Singal, Michael S. Dimitriyev, Sarah E. Gonzalez, A. Patrick Cachine, Sam Quinn, and Elisabetta A. Matsumoto. Programming mechanics in knitted materials, stitch by stitch. *Nat. Commun.*, 15(1):2622, March 2024.
- [14] Guorui Chen, Yongzhong Li, Michael Bick, and Jun Chen. Smart textiles for electricity generation. *Chem. Rev.*, 120(8):3668–3720, 2020.
- [15] Vanessa Sanchez, Conor J. Walsh, and Robert J. Wood. Textile Technology for Soft Robotic and Autonomous Garments. *Adv. Funct. Mater.*, 31(6):2008278, February 2021.
- [16] D. L. Munden. THE GEOMETRY AND DIMENSIONAL PROPERTIES OF PLAIN-KNIT FABRICS. *Journal of the Textile Institute Transactions*, 50(7):T448–T471, July 1959.
- [17] Gamini Lanarolle. Geometry of compact plain knitted structures. *Res. J. Text. Appar.*, 25(4):330–345, November 2021.
- [18] S. Allan Heap, Peter F. Greenwood, Robert D. Leah, James T. Eaton, Jill C. Stevens, and Pauline Keher. Prediction of Finished Weight and Shrinkage of Cotton Knits— The Starfish Project: Part I: Introduction and General Overview. *Text. Res. J.*, 53(2):109–119, February 1983.
- [19] Jonathan M. Kaldor, Doug L. James, and Steve Marschner. Simulating knitted cloth at the yarn level. *ACM Trans. Graph.*, 27(3):1–9, August 2008.
- [20] Georg Sperl, Rosa M. Sánchez-Banderas, Manwen Li, Chris Wojtan, and Miguel A. Otaduy. Estimation of yarn-level simulation models for production fabrics. *ACM Trans. Graph.*, 41(4):1–15, July 2022.

- [21] Xiaoxiao Ding, Vanessa Sanchez, Katia Bertoldi, and Chris H. Rycroft. Unravelling the Mechanics of Knitted Fabrics Through Hierarchical Geometric Representation, July 2023. arXiv:2307.12360 [cond-mat].
- [22] Gabriel Cirio, Jorge Lopez-Moreno, and Miguel A. Otaduy. Yarn-Level Cloth Simulation with Sliding Persistent Contacts. *IEEE Trans. Vis. Comput. Graph.*, 23(2):1152–1162, February 2017.
- [23] Jie Li, Gilles Daviet, Rahul Narain, Florence Bertails-Descoubes, Matthew Overby, George E Brown, and Laurence Boissieux. An implicit frictional contact solver for adaptive cloth simulation. *ACM Trans. Graph.*, 37(4):1–15, 2018.
- [24] Dani Liu, Bahareh Shakibajahromi, Genevieve Dion, David Breen, and Antonios Kontsos. A Computational Approach to Model Interfacial Effects on the Mechanical Behavior of Knitted Textiles. *J. Appl. Mech.*, 85(4):041007, April 2018.
- [25] Jérôme Crassous. Discrete-element-method model for frictional fibers. *Phys. Rev. E.*, 107(2):025003, 2023.
- [26] Tomohiko G Sano, Emile Hohnadel, Toshiyuki Kawata, Thibaut Métivet, and Florence Bertails-Descoubes. Randomly stacked open cylindrical shells as functional mechanical energy absorber. *Commun. Mater.*, 4(1):59, 2023.
- [27] See supplemental material for additional information on the parameters used for simulations.
- [28] B. Audoly, N. Clauvelin, and S. Neukirch. Elastic knots. *Phys. Rev. Lett.*, 99:164301, Oct 2007.
- [29] N. Clauvelin, B. Audoly, and S. Neukirch. Matched asymptotic expansions for twisted elastic knots: A self-contact problem with non-trivial contact topology. *J. Mech. Phys. Solids*, 57(9):1623–1656, 2009.
- [30] M. K. Jawed, P. Dieleman, B. Audoly, and P. M. Reis. Untangling the mechanics and topology in the frictional response of long overhand elastic knots. *Phys. Rev. Lett.*, 115:118302, Sep 2015.
- [31] Widiyanto P. Moestopo, Sammy Shaker, Weiting Deng, and Julia R. Greer. Knots are not for naught: Design, properties, and topology of hierarchical intertwined microarchitected materials. *Sci. Adv.*, 9(10):eade6725, 2023.
- [32] Samuel Poincloux, Mokhtar Adda-Bedia, and Frédéric Lechenault. Crackling dynamics in the mechanical response of knitted fabrics. *Phys. Rev. Lett.*, 121:058002, Jul 2018.